

See discussions, stats, and author profiles for this publication at: <https://www.researchgate.net/publication/277694919>

Synthesis, Characterization, and Self-assembly of Colloidal Quantum Dots

Chapter · February 2012

DOI: 10.1002/9781118311974.ch1

CITATION

1

READS

156

5 authors, including:



Saim Emin

University of Nova Gorica

44 PUBLICATIONS 1,004 CITATIONS

[SEE PROFILE](#)



Alexandre Loukanov

University of Mining and Geology

136 PUBLICATIONS 372 CITATIONS

[SEE PROFILE](#)



Surya Singh

Army Institute of Technology

271 PUBLICATIONS 6,204 CITATIONS

[SEE PROFILE](#)



Seiichiro Nakabayashi

Saitama University

238 PUBLICATIONS 2,589 CITATIONS

[SEE PROFILE](#)

Some of the authors of this publication are also working on these related projects:



Modern Nanotechnology [View project](#)



PEC water splitting [View project](#)

— | —

PART I

INORGANIC MATERIALS

— | —

Synthesis, Characterization, and Self-assembly of Colloidal Quantum Dots

Saim M. Emin¹, Alexandre Loukanov², Surya P. Singh¹, Seiichiro Nakabayashi³ and Liyuan Han¹

¹*Advanced Photovoltaics Center, National Institute for Materials Science (NIMS), Tsukuba, Japan*

²*Laboratory of Engineering Nanobiotechnology, University of Mining and Geology, Sofia, Bulgaria*

³*Department of Chemistry, Faculty of Science, Saitama University, Saitama, Japan*

Abstract

We give a review for the preparation of various types of quantum dots, in which we emphasize general principles through examples that have led to relevant physico-chemical results in this area. Self-assembly procedures of quantum dots are explored because of the unique ways that small objects organize at the nanoscale level.

Keywords: Colloidal quantum dot, self-assembly, surface functionalization

1.1 Introduction

During the past two decades, colloidal semiconductor nanocrystals (also known as quantum dots, abbreviated QDs) have been the subject of intensive research. QDs are of great interest owing to their size-dependent optical properties such as long fluorescence lifetimes, high extinction coefficients, broad absorption spectra, and narrow emission spectra [1]. These properties of QDs enable them to be used in bio-imaging [2], solar cells [3], light-emitting diodes

4 INTELLIGENT NANOMATERIALS

(LEDs) [4], and fluorescence sensing [5]. The earliest studies of QDs, in which the QDs were embedded in glass, date back to 1980s [6, 7]. However, fundamental work initiated in the 1990s on colloidal QDs ultimately led to the development of the synthetic procedures that are currently used to produce QDs with well-defined sizes [8]. Since then, many advances have been made in the development of new QD materials with well-defined morphologies [9].

Mapping of the size-dependent optical properties of QDs is a goal that we share with many researchers. In this chapter, we discuss mainly photophysical studies of type II-VI and IV-VI QDs. To contribute to this fast-growing field, we have systematically explored recent advances in the synthesis and self-assembly of QDs. QDs have been prepared by a variety of methods such as molecular beam epitaxy (MBE) [10], metal–organic chemical vapor deposition (MOCVD) [11], electrochemical deposition [12], and colloidal procedures [13]. Among these methods, colloidal procedures produce QDs with good optical properties and relatively narrow size distributions [14]. Currently developed colloidal routes produce QDs with 10% variation in particle radius and with size control at the 2–5 Å level [15].

Many physical properties of nanometer-scale QDs differ from those observed for their bulk-crystal analogues. Examples of such physical properties include melting points, charging energies, and bandgap alignment. Nevertheless, the size-dependent shifts observed in QDs' absorption and photoluminescence spectra are what make them attractive for widespread use [16]. In this chapter, we describe methods for preparation of QDs with well-defined sizes and optical properties. Furthermore, we survey techniques for the self-assembly of QDs on liquid and solid surfaces. In particular, the self-assembly of QDs onto solid substrates is discussed as it pertains to the preparation of optoelectronic devices [17].

1.2 Size-dependent Optical Properties of Quantum Dots

Size-dependent fluorescent emission is one of the most important features of colloidal QDs. On the basis of this property, various fluorescent probes have been designed for tissue labeling [18–20], tumor cell detection [21], or fabrication of multicolor LED devices [22]. Figure 1.1a shows a series of luminescent CdSe nanocrystals

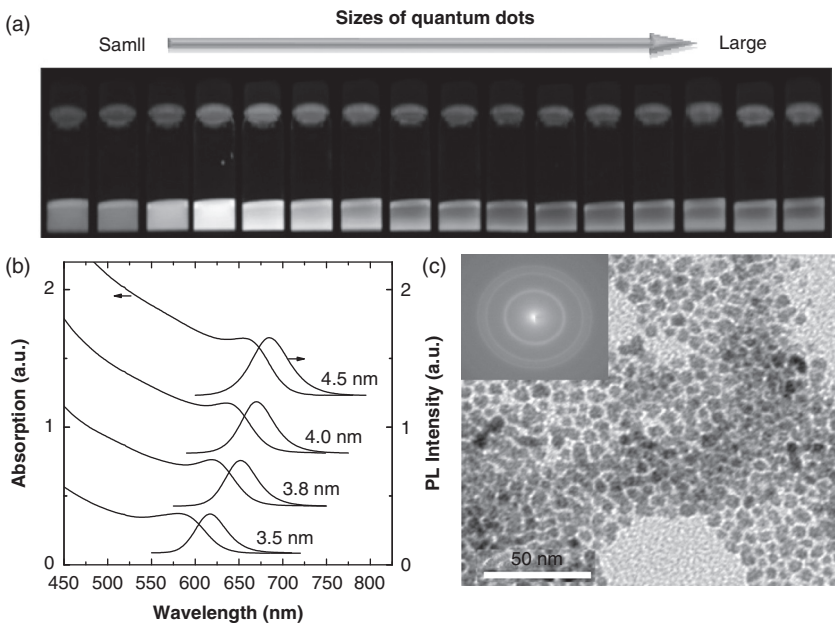


Figure 1.1 (a) Photoluminescence of CdSe QD samples exposed to ultraviolet light. (b) Absorption and PL spectra of CdTe QDs with varying sizes as indicated for each sample. (c) TEM image of a film composed of spherical CdTe QDs. The inset in (c) is a selected area electron diffraction (SAED) pattern from the QD film. Reprinted from refs. [23, 24].

prepared by means of colloidal procedures [23]. As a general rule, the size-dependent emission is attributed to the QDs' band gap, which causes a shift in the absorption and photoluminescence (PL) spectra (Fig. 1.1b) [24]. This phenomenon, which is unique to QDs and is not observed in analogous bulk semiconductor crystals, can be explained with quantum-mechanical models and is discussed further below. Typical sizes of colloidal QDs are on the order of several nanometers as revealed by transmission electron microscopy (TEM; Fig. 1.1c).

In a bulk semiconductor, an electron can be excited from the valence band to the conduction band by absorption of a photon with an appropriate energy. The excited electron in the conduction band leaves behind a positive hole in the valence band. This electron–hole pair, called an exciton, has its lowest energy state slightly below the lower edge of the conduction band, and its wavefunction extends over a large distance. The average separation

6 INTELLIGENT NANOMATERIALS

distance between the electron and hole in an exciton is referred to as the Bohr radius; the Bohr radius differs among materials [25]. In a bulk semiconductor, the dimensions of the crystal are much larger than the exciton Bohr radius, allowing the exciton to extend to its natural limit. In terms of electron energy levels, this condition corresponds to a continuous band structure. However, if the size of a semiconductor crystal becomes small enough that it approaches the length of the exciton Bohr radius, then the electron energy levels are greatly affected. In that case, the energy levels are treated as discrete, meaning that there is a small and finite separation between the energy levels. This phenomenon is called the “quantum confinement effect” [26], and its theoretical treatment is usually based on the quantum mechanical particle-in-a-box approach [27]. For example, the Bohr exciton radii in bulk CdS and CdSe are approximately 3 and 5 nm, respectively; therefore, the quantum confinement effect is observed in CdS and CdSe QDs with sizes near those Bohr radii [28]. It is useful to compare the dimensions of QDs with their Bohr radii in order to estimate the quantum confinement regime. In general, the Bohr radius of a particle is given as [29]

$$a_B = \frac{\epsilon m a_0}{m^*} \quad (1.1)$$

where ϵ is the dielectric constant of the material; m^* is the reduced mass of the electron–hole pair; m is the electron mass, 9.109×10^{-31} kg; and a_0 is the Bohr radius of the hydrogen atom.

For nanocrystals, it is convenient to consider three different Bohr radii: one for the electron (a_e), one for the hole (a_h), and one for the exciton (a_{exc}). With these Bohr radii, three different confinement regimes can be considered [30]. The first of these is the *strong confinement regime*, which occurs when the nanocrystal radius, R , is much smaller than a_e , a_h , and a_{exc} (i.e., $R < a_e, a_h, a_{exc}$). The second is the *intermediate confinement regime*, which occurs when R is between a_e and a_h (i.e., when $a_h < R < a_e, a_{exc}$). Finally, the third case is the *weak confinement regime*, which occurs when R is larger than both a_e and a_h , but is much smaller than a_{exc} (i.e., when $a_e, a_h < R < a_{exc}$). The confinement regime depends on the type of semiconductor material and the size of the nanocrystal. For example, because the Bohr radius (exciton length) in CuBr is ~ 1.2 nm (Table 1.1), and synthesized CuBr nanocrystals are typically larger than this size, those nanocrystals are in the weak confinement regime.

Table 1.1 Physical data for various semiconductors (adapted from ref. [31]).

Semiconductor	Bandgap Energy (eV)	Electron Effective Mass m_e/m_0^*	Hole Effective Mass m_h/m_0^*	Exciton Bohr Radius, a_B (nm)
CdS	2.58	0.24	0.70	2.8
CdSe	1.84	0.13	0.45	4.9
CdTe	1.60	0.10	0.40	~7
ZnSe	2.82	0.15	0.81 / heavy hole	3.8
CuBr	3.07	0.25	1.40 / heavy hole	1.2
CuCl	3.39	0.40	2.40 / heavy hole	0.7

Two detailed theoretical approaches are used to predict the exciton energies in QDs: the effective mass approximation (EMA) model [31] and the tight-binding model [32]. In this chapter, a brief description is given only for the EMA model owing to its simplicity.

1.2.1 Band Gap Energies

The EMA model is based on the particle-in-a box approach, which was first proposed by Efros *et al.* [30] and later modified by Brus [7]. The model assumes a particle in a potential well with an infinite potential barrier at the particle boundary. For a free particle (electron or hole) to assume any position in the box, the relationship between the particle's energy (E) and wave vector (k) is given as

$$E = \frac{\hbar^2 k^2}{2m^*} \quad (1.2)$$

where m^* is the reduced mass of the exciton, and \hbar is the Plank's constant.

8 INTELLIGENT NANOMATERIALS

For a direct semiconductor, delocalized electron (or hole) waves follow a quadratic relationship and give rise to parabolic curves near the band edges (Fig. 1.2a). For example, because CdSe is a direct semiconductor, both its valence-band maximum and conduction-band minimum occur at $k = 0$. Physically, the EMA model attempts to incorporate the complicated periodic potential felt by the charge carrier in the crystal lattice. This model allows the semiconductor atoms in the lattice to be completely ignored and the electron and hole to be treated as if they were free particles, but with a different mass. This simple method can be improved by incorporating the $\mathbf{k} \bullet \mathbf{p}$ approach, which allows obtaining analytical expression for the band energies to second order in k [33]. From the EMA method, the electronic properties of a QD can be determined by simply considering the modification of the energy of the charge carriers: this consideration is achieved by solving the Schrödinger equation for a particle in a three-dimensional box. However, analytical solutions for the Schrödinger equation are difficult because center-of-mass motion and reduced mass motion cannot be separated as independent coordinates. Various approaches have been used to solve this problem including the perturbation theory of Brus *et al.* [34]. On the basis of Brus's approach, the lowest energy separation between the hole and electron states in a QD is given as

$$E_{\min} = \frac{\hbar^2 \pi^2}{2R^2} \left[\frac{1}{m_e^*} + \frac{1}{m_h^*} \right] - \frac{1.8q^2}{\epsilon R} - 0.25E_{\text{Ryd}}^* \quad (1.3)$$

where R is the radius of the QDs, m_e^* is the effective electron mass, m_h^* is the effective hole mass, ϵ is the dielectric constant, q is the elementary charge, and E_{Ryd} is the Rydberg energy. The first term in Eq. 1.3 represents the quantum confinement energy, whereas the second term shows the Coulomb interaction energy. Finally, the last term gives the Rydberg energy, which is size-independent and usually can be neglected in QDs with small dielectric constants [35]. E_{\min} is often referred to as the bandgap of the QD since this value represents the threshold energy for photon absorption, which is blue-shifted from the bulk bandgap, E_g . Equation 3 predicts that the size-dependent exciton energy increases as the size of the QD crystallite is reduced (Fig. 1.2c). Although the EMA model explains the exciton energies of large nanocrystals, it fails to accurately predict the energies of small QDs with sizes below 5 nm (Fig. 1.2c).

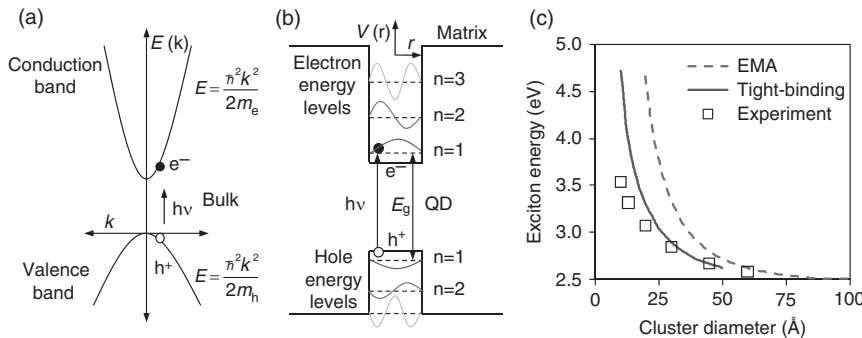


Figure 1.2 (a) Band diagram for a two-band model for direct bulk semiconductors. (b) Scheme of QD discrete energy levels. The only states (n) are those whose wavefunctions (colored lines) vanish at the borders of well. (c) The dependence of the optical bandgap (exciton energy) of CdS on QD cluster size. Squares are experimental data, dashed red lines represent EMA calculations, and solid blue lines are from tight-binding calculations. (c) Reproduced from ref. [35].

To adequately approximate exciton energies for those small QDs, tight-binding calculations are required [36].

1.2.2 Absorption Spectra

The most useful information about quantum confinement in QDs can be obtained from their absorption spectra [37]. The observed blue-shift in these spectra contains relevant information about the bandgap energies as already mentioned above. Generally speaking, the observed peaks in an absorption spectrum are characteristic of certain optical transitions. For example, a relatively sharp feature near the onset of 640 corresponds to the lowest excited state of CdSe QDs and is referred to as an excitonic peak (Fig. 1.3). This transition, abbreviated as $1S_{3/2}-1S$, is used to calculate the size of the QD by employing methods such as EMA [39]. Whereas the position of this transition depends on the bandgap (particle size), the spectral shape and width are strongly influenced by the size distribution of the QDs [38]. In general, comparisons between experimentally obtained absorption spectra and calculated optical transitions show good agreement [40]. A commonly used notation for the optical transitions labels the electron states as nL and the hole states as nL_F [41, 42]. In these notations, n is the principal quantum number (1, 2, 3,...etc.), L is the orbital angular momentum of the envelope wave function (S, P, D,...etc.), and F is the total angular momentum

10 INTELLIGENT NANOMATERIALS

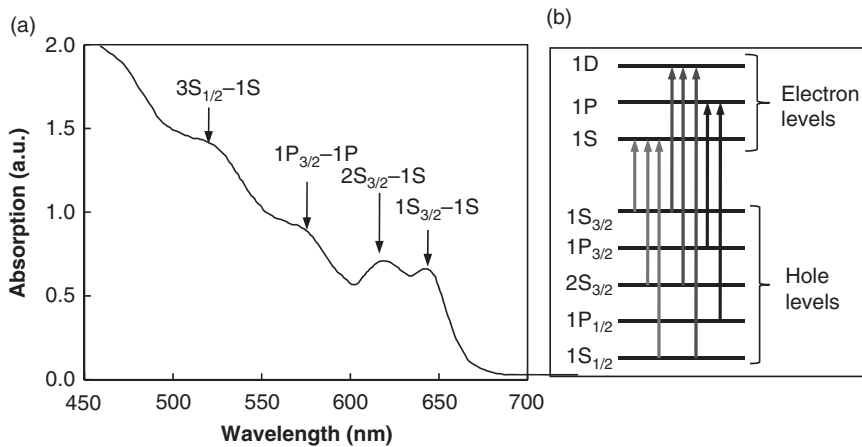


Figure 1.3 (a) Absorption spectrum of CdSe QDs. (b) Scheme illustrating the allowed optical transitions in CdSe QDs ($R = 2.5$ nm) between the lowest electron and hole levels. Reproduced from ref. [39].

($F = 2L + S$), where S is the spin, and the projection of F along a magnetic axis is $m_F = -F$ to $+F$. Thus electron states become $1s$, $2s$, $1p$, etc., and hole states become $1S_{1/2}$, $1S_{3/2}$, $1P_{1/2}$, etc. The hole states are $(2F + 1)$ -fold degenerate. This degeneracy is lifted if (a) the QD crystal structure is a hexagonal lattice; (b) the QDs are nonspherical [43]; and (c) the electron hole (e-h) exchange interaction [44] is taken into account, leading to a fine structure of the lowest exciton. For optical transitions in ideal spherical QDs, the selection rules are $\Delta n = 0$; $\Delta L = 0, \pm 2$; and $\Delta F = 0, \pm 1$. These rules can be broken by QDs that are nonspherical and by strong hole-state mixing.

1.3 Procedures for Synthesis of Colloidal Quantum Dots

Many documented procedures exist for the preparation of colloidal QDs, but we restrict our discussion in this chapter to “wet chemistry” synthetic routes. All the procedures described below are well established for the preparation of II–VI and IV–VI QDs.

1.3.1 Synthesis of Quantum Dots in Reverse Micelles

Reverse micelles are thermodynamically stable, nanoscopic formations formed in the presence of a solute, a solvent, and a surfactant.

Typical micelles are tiny water droplets dispersed in an oil phase and surrounded by surfactant molecules ($d_{\text{micelle}} \sim 5 \text{ nm}$). Close packing of the surfactant polar heads oriented toward the aqueous medium allows low interfacial tension between the water and oil phases to be maintained, resulting in the long-term stability of reverse micelles [45]. Moreover, reverse micelles have been studied by various methods such as dynamic light scattering (DLS) [46], small-angle X-ray scattering (SAXS) [47], and small-angle neutron scattering (SANS) [48]. Through these techniques, the relationship between reverse micelle sizes and morphologies has been established [49].

During the last several decades, reverse micelles have been used as ideal templates for preparation of various metal and semiconductor nanoparticles [50]. Two popular micellar systems work well for preparation of metal and semiconductor nanoparticles [51]. One such micellar system contains a surfactant called bis(2-ethylhexyl) sulfosuccinate (AOT). AOT reverse micelles are widely used for QD preparation because they produce relatively monodisperse QDs [52]. Figure 1.4 shows absorption spectra and a TEM image of CdSe QDs synthesized in AOT micelles [53]. The absorption

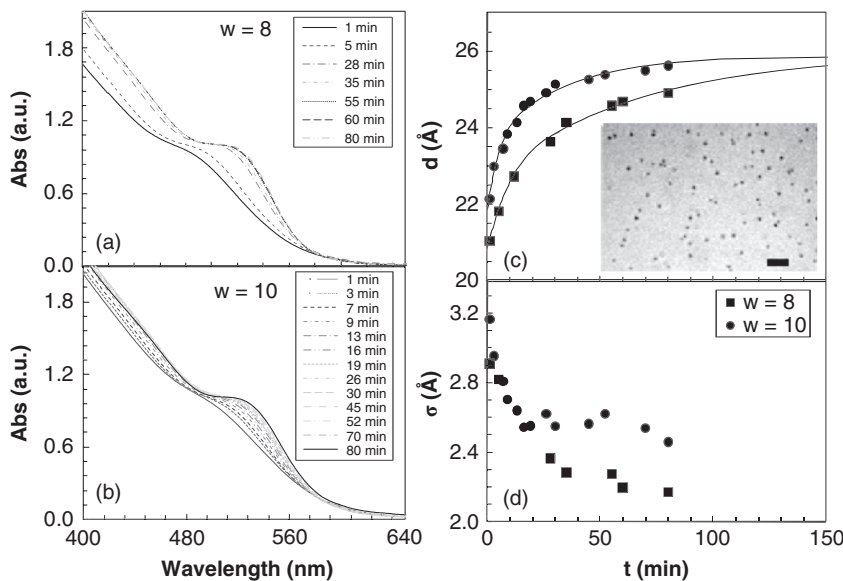


Figure 1.4 (a, b) Absorption spectra of CdSe QDs synthesized in AOT reverse micelles at varying $w = [\text{H}_2\text{O}]/[\text{surfactant}]$. (c, d) Temporal changes in (c) sizes of QDs and (d) polydispersity of QDs. Reprinted from ref. [53].

12 INTELLIGENT NANOMATERIALS

spectra were recorded at different reaction times. The second micellar system uses the surfactant cetyltrimethylammonium bromide (CTAB). Using this surfactant, Emin *et al.* have studied the growth kinetics of CdS QDs in a water/CTAB+4-pentenol/benzene system [13]. This surfactant has only one alkyl chain in its structure, and its use in reverse micelles requires the addition of a co-adsorbent during micelle preparation. In general, reverse micelles composed of AOT surfactant produce QDs with better optical properties than those produced by means of the CTAB system. From these two surfactants, various QDs have been synthesized including CdS [54–56], CdSe [57], PbS [58], CdS(core)/ZnS(shell) [59], and others. In summary, reverse micelles can control the dimensions of QDs. One disadvantage of micellar systems is that the fluorescence quantum yields of QDs produced from micelles are relatively low compared with yields of QDs produced by aqueous and hot-matrix procedures.

1.3.2 Synthesis of Quantum Dots in Aqueous Media

The first steps toward realizing successful aqueous alternatives to the organometallic synthesis of QDs have been undertaken by Nozik's and Wellers's groups, both of whom have synthesized CdTe QDs [60, 61]. In later studies, Rogach *et al.* have demonstrated that CdTe QDs capped with thioglycolic and 3-mercaptopropionic acids can be prepared from inexpensive reagents and in large quantities [62], thus making these QDs advantageous for practical applications. Other capping molecules may also be used with CdTe QDs, with successful examples including L-cysteine [63], glutathione [64], dimethylaminoethanethiol [65], dihydrolipoic acid [66], or mercaptosuccinic acid [67]. Capping-molecule functional groups such as –COOH, –NH₂, or –OH are chosen on the basis of the QDs' ultimate application. For example, amino acid capping molecules (e.g., glutathione) are used to enhance the biocompatibility of QDs [68]. The above-mentioned capping molecules can be used not only with CdTe QDs but also with other types of QDs such as ZnSe [69], ZnSe(core)/ZnS(shell) [70], CdS [71], CdSe [72], Cd_xHg_{1-x}Te [73], or HgTe [74].

Though CdTe QDs prepared in aqueous environments are highly luminescent, CdS and CdSe QDs exhibit low PL quantum yields. This phenomenon is explained by photo induced hole transfer from the mercapto group to CdS (or CdSe) QDs [75]. This photoinduced

hole transfer is absent from the CdTe QD system, thus allowing high PL quantum yields (~50%) to be achieved. Moreover, the nature of the capping molecules used in CdTe QDs can affect the PL quantum yield [76]. For example, amino-thiols such as cystamine provide a moderately high PL quantum yield, whereas others such as 3-mercaptopropionic acid provide a higher PL quantum yield [77]. The difference in the PL quantum yield is attributed to defect states in the CdTe QDs rather than to hole transfer as mentioned above. Figure 1.5a shows typical absorbance and PL spectra of CdTe QDs capped with 3-mercaptopropionic acid (MPA). The effect of QD size on PL quantum yield is also shown (Fig. 1.5b). The transient PL clearly improves with increasing QD size, leading to longer relaxation lifetimes. The latter phenomenon is caused by defect states at the surface of the QDs.

Currently, the safe handling of nanometer-sized materials is an issue of great concern [78]. Toward this end, researchers have explored the preparation of QDs from low-toxicity materials, as well as environmentally friendly preparation methods [79] such as the preparation of ZnSe QDs in water [80]. The synthetic procedure

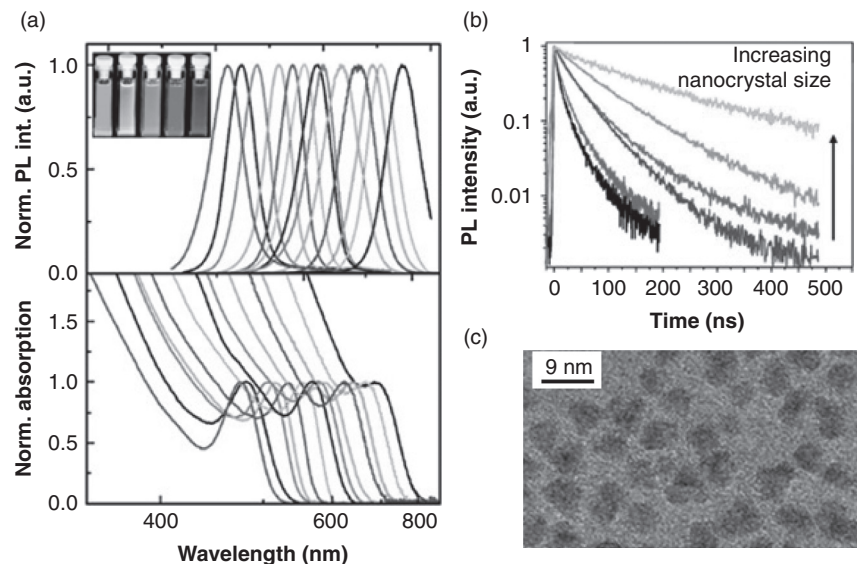


Figure 1.5 (a) Photoluminescence (top) and absorption spectra of CdTe QDs capped with mercaptopropionic acid (MPA). (b) PL decays of MPA-capped CdTe QDs of increasing sizes. (c) High-resolution TEM image of CdTe QDs. Reprinted with permission from ref. [62].

14 INTELLIGENT NANOMATERIALS

for these ZnSe QDs is similar to that used for synthesis of CdTe QDs [81]. To improve the PL properties of these ZnSe QDs, colloidal solutions are often irradiated with visible light [82] or alternatively with ultraviolet light [83]. In general, aqueous syntheses provide a convenient means of QD preparation. Nevertheless, the kinds of capping molecules that can be used in an aqueous approach are limited [84], and aqueous synthesis is further limited to the preparation of QDs with hydrophilic ligands.

1.3.3 Hot-matrix Synthesis of Quantum Dots

The most successful methods for preparation of II-VI and III-V QDs involve the pyrolysis of metal-organic precursors in hot coordinating solvents [85]. For example, to synthesize CdSe QDs, a metal precursor (e.g., dimethylcadmium) and a chalcogenide precursor (e.g., TBP=Se) are reacted at about 300°C [86]. In recent years, these “hot-matrix” synthetic schemes have been modified, and hazardous precursors like dimethylcadmium have been replaced with safer alternative compounds such as cadmium stearate [87]. These changes allow the reaction temperature to be lowered to about 150°C [88]. Moreover, the surfactant trioctylphosphine oxide (TOPO), which serves as a solvent and coordinating medium, has been replaced with noncoordinating solvents like paraffin and 11-octadecene (ODE) [89]. By using noncoordinating solvents in hot-matrix methods, it is possible to obtain QD samples with 5% standard deviation from the mean size [90]. In addition, the use of these less expensive reagents in hot-matrix syntheses allows for scale-up and lower-cost production of QDs.

1.4 Types of Semiconductor Quantum Dots

Depending on the capping agents, colloidal semiconductor nanocrystals are divided into several groups. The first group includes binary QDs that are coated with organic molecules such as trioctylphosphine [91] or alkanethiols [92]. The second group consists of QDs with core/shell structures. Usually, a core semiconductor (e.g., CdS, CdSe) is covered with a shell of inorganic semiconductor material (e.g., ZnS, CdTe). In general, the growth of an inorganic shell on a core requires close lattice matching between the core and shell semiconductors. Moreover, core/shell QDs can be also capped with organic molecules in order to stabilize the QDs in

various solvents. Figure 1.6 shows illustrations of various types of QDs and their respective energy diagrams.

The relative band offsets between the core and shell semiconductor materials can further split the core/shell QDs into subgroups such as type-I, type-II, or multishell QDs. Examples of type-I QDs are CdS(core)/ZnS(shell) [93] and CdSe(core)/ZnS(shell) [94]. Such structures are designed because, upon illumination, the electron-hole pair is confined in the core material, thus allowing a high PL quantum yield to be achieved. This property of type-I QDs is exploited in fluorescence imaging [95] and in light-emitting devices [96]. The second subgroup of core/shell-structured QDs is type-II QDs. Examples of type-II QDs include CdSe(core)/CdS(shell) [97], CdSe(core)/CdTe(shell) [98], CdS(core)/CdSe(barrier)/CdSe(shell) [99], and others. These materials are designed to enable efficient charge separation in optoelectronic devices [100].

1.4.1 Binary Quantum Dots

Research on binary semiconductor QDs was initiated in the early 1980s [101]. However, detailed studies of these QDs began only when hot-matrix synthetic methods were introduced in 1990. Among binary QDs, detailed studies have been devoted to ZnS [102], ZnSe [103], CdS [104], CdSe [105], CdTe [106], PbS [107], InP [108], and GaAs [109]. From an application point of view these QDs require

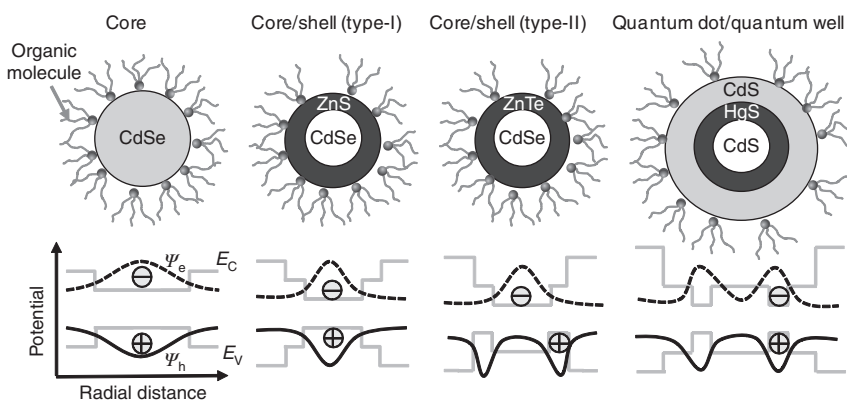


Figure 1.6 Illustrations of various types of QDs (top), and potential energy diagrams for the respective QDs' electrons and holes (bottom). The dashed and solid black lines illustrate the electron (Ψ_e) and hole (Ψ_h) wavefunctions, respectively.

16 INTELLIGENT NANOMATERIALS

coating molecules to permit solubility in certain solvents. However, such organic coating often affects the optical properties of the QDs. Whereas molecules such as TOPO preserve the luminescence of QDs, other molecules like hexanethiol quench their luminescence [110]. To preserve the luminescence of binary QDs, they need to be coated either with an appropriate organic capping layer or with an inorganic semiconductor shell. Coating of QDs with a second layer of inorganic material allows better passivation of surface defects and improves the PL quantum yield. Binary QDs are useful for studying and elucidating fundamental photophysical phenomena [111].

1.4.2 Alloyed Quantum Dots

Alloyed QDs also have received much attention. This type of QD offers unique optical properties such as continuous tuning of quantum confinement without the need to change the size of the QD. Figure 1.7 shows absorption and PL spectra of alloyed $\text{Hg}_x\text{Cd}_{1-x}\text{Te}$ QDs, which have tunable emission in the range from 500 to 950 nm that is achieved by varying the stoichiometry of mercury [112]. This tunable emission is ascribed to the lower exciton mass in $\text{Hg}_x\text{Cd}_{1-x}\text{Te}$ QDs compared to that of binary CdTe QDs. In alloyed QDs, control over the quantum confinement effect can be achieved in two ways. The first way is by varying the particle size, as is done for binary QDs, and the second way is through modulation of the composition of alloyed QDs. Typical examples of alloyed QDs include $\text{CdSe}_x\text{Te}_{1-x}$ [113], $\text{Zn}_{1-x}\text{Cd}_x\text{S}$ [114, 115], and $\text{Zn}_{1-x}\text{Cd}_x\text{Se}$ [116]. Alloyed nanocrystals based on CdTe usually emit light in the near-infrared region,

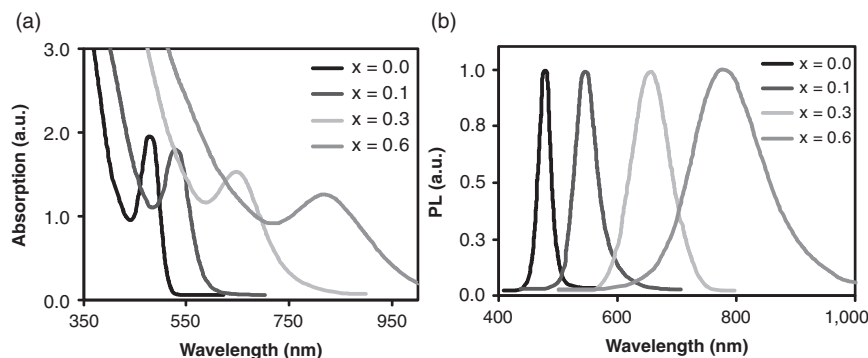


Figure 1.7 (a) Absorbance and (b) PL spectra of $\text{Hg}_x\text{Cd}_{1-x}\text{Te}$ QDs ($d = 2.3$ nm) with varying Hg stoichiometry. Reproduced from ref. [112].

making them ideal candidates for *in-vivo* molecular imaging [117] and biolabeling [118]. In comparison with conventional organic fluorophores, near-infrared QDs should allow more-sensitive *in-vivo* detection since near-infrared light can penetrate deeper into the internal organs of living animals.

1.4.3 Core/shell Quantum Dots: “Type-I”

Type-I colloidal QDs are designed with the purpose of achieving high fluorescence quantum yields [119, 120]. A typical example of a type-I QD is CdSe(core)/ZnS(shell) [121]. With PL emission wavelengths that are tunable throughout the visible-light region, CdSe QDs are ideal for fluorescence studies [122]. However, in the absence of a protective shell, CdSe QDs usually exhibit low PL quantum yields. To improve CdSe QDs’ luminescence, they need to be coated with a layer of a wider-bandgap material such as ZnS. This ZnS coating passivates the CdSe QDs’ surface defects, which cause nonradiative recombinations and thus lower the PL quantum yield. Moreover, the ZnS coating layer also confines photogenerated electron–hole pairs within the CdSe QDs. Confining excitons within the CdSe QDs promotes radiative recombination, which results in an increased PL quantum yield (~50%) [123]. Evidence of ZnS shell formation on CdSe QDs has been examined by various techniques. Vinyakan *et al.* evaluated the thickness of the ZnS layer on CdSe QDs by means of fluorescence spectroscopy [124]. In their study, a phenothiazine electron donor was used to probe the photoinduced hole transfer from phenothiazine to CdSe/ZnS QDs. By varying the thickness of the ZnS shell on the CdSe core, they found that the rate of hole transfer from phenothiazine to CdSe was proportional to the thickness of the ZnS shell. These findings show that the layer of ZnS on CdSe QDs is nonuniform. Yu *et al.* reached a similar conclusion by employing scanning transmission electron microscopy (STEM) coupled with electron energy loss spectroscopy (EELS) [125]. Figure 1.8 shows the resulting STEM images of CdSe QDs and corresponding chemical distribution spectra taken at various locations. EELS was used to study the shell distribution in CdSe/ZnS QDs by collecting localized core–edge EELS spectra on the sub-nanometer scale. The authors concluded that ZnS shell distribution on CdSe QDs is nonuniform and may reflect differences in chemical activity of these QDs. These two studies provide insight on the shell distribution in core/shell QDs and also

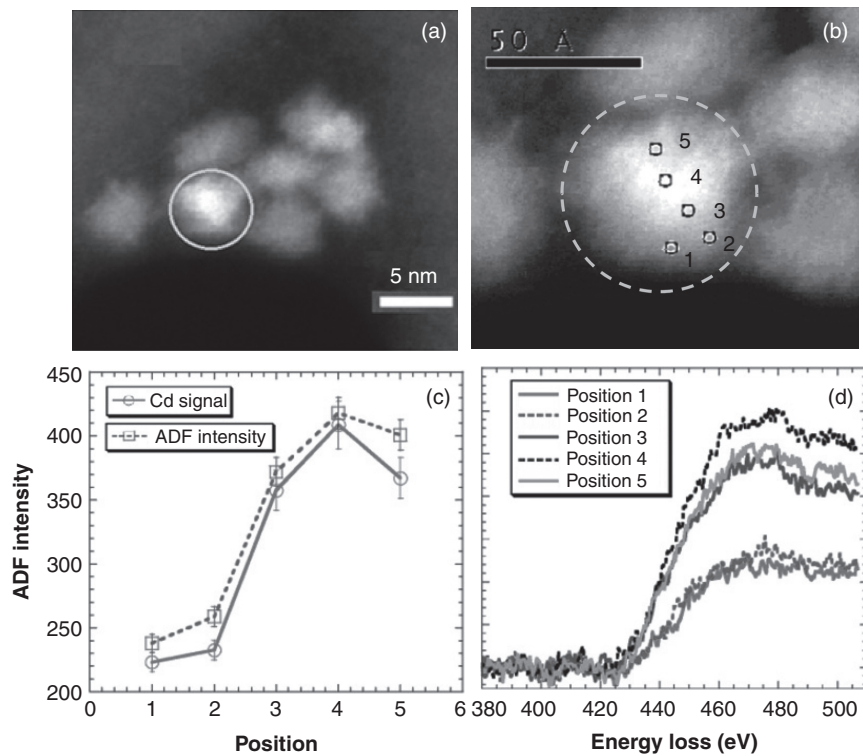


Figure 1.8 (a-b) Annular dark field (ADF) STEM images of CdSe/ZnS QDs at different magnifications. Elemental distribution (c) and electron loss spectra (d) for Cd at different locations as shown in (b). Reprinted from ref. [125].

demonstrate that shell formation is anisotropic. Since close lattice matching between the core and shell is required for epitaxial shell growth, these results suggest that the lattice mismatch (10.6%) [126] between CdSe and ZnS materials may cause the observed nonuniform shell distribution. In conclusion, type-I QDs are attractive for PL studies, and the shell thickness of these materials greatly affects their optical properties.

1.4.4 Core/shell Quantum Dots: “Type-II”

Examples of type-II QDs include CdS(core)/CdTe(shell) [127], CdSe/CdTe [128], CdTe/CdSe [129], CdTe/CdS [130], CdSe/ZnTe [131], CdS/PbS [132], and InAs/CdSe [133]. These materials are attractive because they emit at wavelengths that are not accessible

with binary QDs. Type-II QDs have been studied because of their slow recombination lifetimes, which have important applications in optoelectronic devices [134] and fluorescence imaging [135]. In type-II QDs, the conduction and valence band levels of the cores are offset from those in the shells. This offset allows charge carriers to reside on opposite sides of the core/shell structure under illumination. Therefore, electron–hole recombination takes place at the interface of the two semiconductors, leading to slow recombination lifetimes. For example, whereas binary CdTe QDs exhibit excited state lifetimes on the order of 18 ns, CdSe/ZnSe QDs with 6 monolayers of ZnSe shell show PL lifetimes that are 7 times as long (~115 ns) [136]. Moreover, CdSe/ZnSe QDs display tunable emission from 500 to 900 nm. In general, both the shell thickness and the core size affect the observed changes in the optical properties. The shell formation in core/shell QDs can be studied by X-ray diffraction or by TEM. Figure 1.9 shows clear evidence of shell formation on CdTe QDs. The shift of the CdTe diffraction peak toward that of ZnSe illustrates that the cores are covered with a shell of ZnSe. Further evidence of ZnSe shell growth can be observed in the differences in the QDs' lattice constants before and after shell growth.

Another model system of a type-II QD structure that has been extensively studied is CdTe (core)/CdSe(shell) [137]. For this system, holes are mostly confined to the CdTe core, whereas electrons are mostly confined to the CdSe shell. CdTe/CdSe QDs exhibit tunable emission in the range of 700 to 1000 nm and have slow recombination lifetimes (~57 ns). These QDs can be used for time-gated fluorescence imaging [138] or as near-infrared-emitting materials for *in-vivo* imaging [139].

1.4.5 Quantum Dot/quantum Well Nanocrystals

Core/shell QD preparation methods have been extended to the preparation of quantum dot/quantum well (QDQW) structures [140]. This type of QD has been used in light-emitting diodes (LEDs) [141, 142]. Well-known examples of QDQW nanostructures include ZnS(core)/CdS(barrier)/ZnS(shell) [143], CdS/HgS/CdS [144, 145], and CdSe/ZnS/CdSe [146, 147]. Among these nanocrystals, CdS/HgS/CdS QDQWs have been used as a prototype for numerous investigations including transient absorption studies [148], high-resolution TEM studies [149], and optically detected magnetic resonance spectroscopy [150]. In principle, QDQW

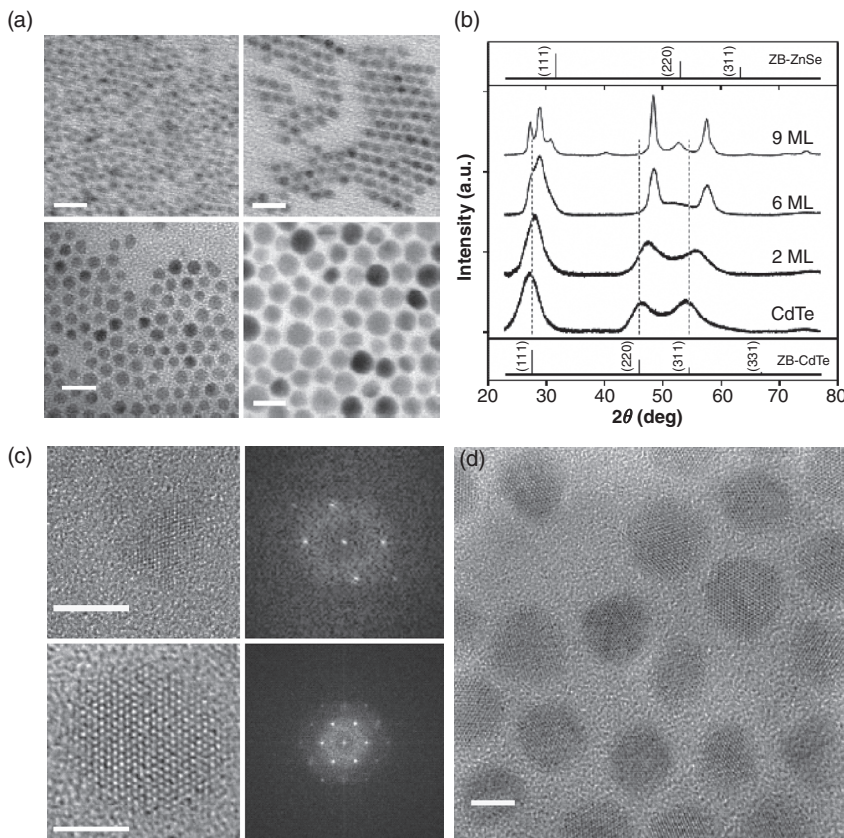


Figure 1.9 (a) Transmission electron microscopy (TEM) images of CdTe QDs (top left) and CdTe/ZnSe QDs with shell thicknesses of 2 (top right), 6 (bottom left), and 9 (bottom right) monolayers. (b) X-ray diffraction spectra of CdTe and CdTe/ZnSe QDs. (c) High-resolution TEM images along with Fourier transform images of CdTe and CdTe/ZnSe QDs. (d) High-resolution TEM image of CdTe/ZnSe QDs with a shell thickness of 6 monolayers. Scale bars: (a) 20 nm, (c) 5 nm, and (d) 5 nm. Reprinted with permission from ref. [136].

structures exhibit unique dual light emission. This property of QDQW has recently been exploited by Nizamoglu *et al.* for the preparation of a white LED device [151]. The heterostructure of the QDQWs used in that study consisted of a quantum dot core made of CdSe ($\lambda_{\text{em}} \sim 600$ nm), a ZnS shell barrier surrounding the core, and finally a CdSe quantum well ($\lambda_{\text{em}} \sim 550$ nm) surrounding the ZnS barrier layer. Figure 1.10 shows a typical PL spectrum obtained from CdSe/ZnS/CdSe QDQW nanoparticles. The dual emission

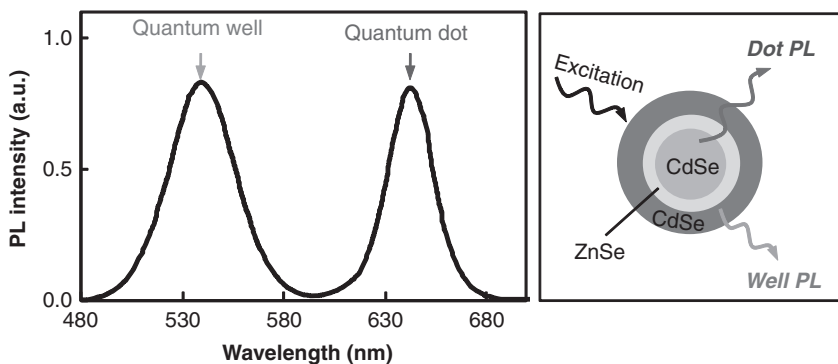


Figure 1.10 PL spectrum and schematic structure of CdSe/ZnSe/CdSe QDQW. Reproduced from ref. [146].

peaks are achieved because the core and the shell emit light simultaneously. Similar results are observed for a CdS/HgS/CdS QDQW system as well. Experimental and theoretical calculations reveal the origin of the dual emission. For example, in the CdS/HgS/CdS QDQW system, both electron and hole can penetrate in the potential well, thus allowing a second PL peak to emerge from the quantum well at shorter wavelengths [152]. The QDQW structures presented here could be of great interest as dual emitting fluorophores in bio-imaging studies.

1.4.6 Transition-element-doped Quantum Dots

In addition to the structures introduced above, there is a class of QDs referred as doped QDs [153]. Incorporation of dopant ions into the crystal lattice structure of a colloidal semiconductor QD creates novel magnetic and magneto-optical properties [154]. Examples of doped QDs include Mn²⁺-doped ZnSe (ZnSe:Mn) [155], Mn²⁺-doped CdSe [156], Cu²⁺-doped ZnSe [157], and Co²⁺-doped ZnSe [158]. These materials have been intensively studied owing to their unique steady-state and transient PL spectra (Fig. 1.11). In general, doping of QDs allows access to dual emission and long fluorescence decays [159]. Doped nanocrystals emit a range of colors in contrast to undoped host QDs and also exhibit higher resistance to photo-oxidation [160].

Semiconductors (bulk or nanoparticulate) that are doped with magnetic ions are characterized by an *sp-d* exchange interaction

22 INTELLIGENT NANOMATERIALS

between the host and the dopant [161]. Specifically, strong interactions appear between electron and hole spins of the host and those of the dopant ions. Photoluminescence in doped QDs typically involves two general cases. The first scenario appears in ZnS:Mn and ZnSe:Mn QDs, where the shift between absorption and PL maxima arises from rapid (~ 5 ps) energy transfer from the excited semiconductor to the Mn^{2+} dopant [162]. The energy of photoexcited electrons is released into the dopant lattice, causing an internal d-d transition in the dopant (Fig. 1.11b). For example, in Mn^{2+} ions this transition is assigned to ${}^4T_1 \rightarrow {}^6A_1$, which results in very slow decays (~ 100 μ s) [163]. The second scenario appears in CdSe:Mn and in CdTe:Mn QDs, where the lowest excitonic states occur below the Mn^{2+} d-d excited states (Fig. 1.11c). In this case, the PL transitions usually are characterized by exciton spin polarization and spontaneous magnetization of the Mn^{2+} spin under the exciton exchange field [164]. Figure 1.11d clearly illustrates these two cases in ZnSe:Mn and ZnSe:Mn/ZnCdSe QDs.

From an applications point of view, doped nanocrystals may eliminate toxicity problems previously encountered with cadmium-based QDs in bio-imaging studies, because some types of doped QDs (*e.g.* ZnSe:Mn) are made of less-harmful elements than those

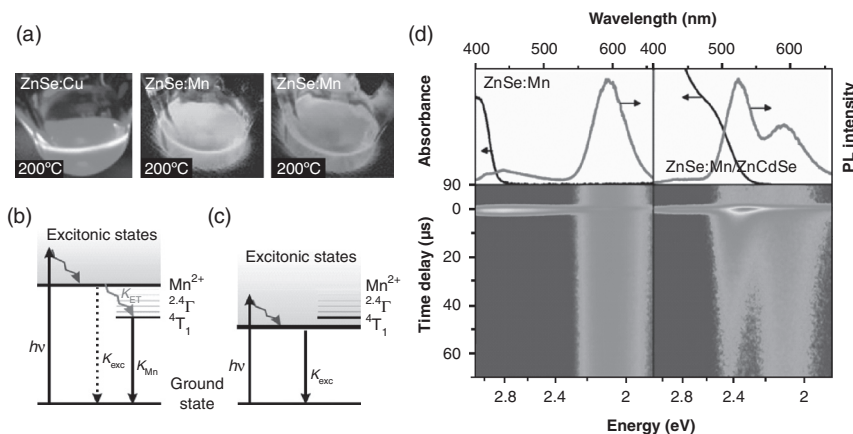


Figure 1.11 (a) Fluorescence of Mn^{2+} - and Cu^{2+} -doped ZnSe QDs. (b, c) Illustrations of electronic structure related to PL in (b) Mn^{2+} -doped ZnSe and (c) Mn^{2+} -doped CdSe QDs. (d, top) Room temperature absorption and photoluminescence spectra of ZnSe:Mn (left) and ZnSe:Mn/ZnCdSe (right) nanocrystals. (d, bottom) Transient photoluminescence plots for the same samples. Reprinted with permission from ref. [163].

that are currently used in bio-imaging [165]. Dual emission from doped QDs may also allow for better resolution in bio-imaging. In addition, doped QDs are also actively studied in LED devices for the generation of white light [166].

1.5 Surface Functionalization of Quantum Dots

To utilize colloidal QDs in various fields, suitable capping agents are needed. Capping layers with specific functional groups allow QDs to be dispersed in different media. For example, preparation of water-dispersible QDs can be accomplished electrostatically with small charged ligands [167], amphiphilic triblock copolymers [168], functionalized oligomeric phosphines [169], amphiphilic saccharides [170], or silica [171]. Although small ligands promote facile synthesis and allow preparation of QDs with small hydrodynamic radii, they also suffer from disadvantages such as coagulation of nanoparticles in buffer solutions or in biological matrices [172]. In contrast, QDs covered with amphiphilic triblock copolymers have larger hydrodynamic radii. Moreover, triblock copolymers allow the QDs to maintain high PL quantum yields in water [173]. Typically, the spectroscopic features of QDs are governed mainly by the capping layer and by the QDs' microenvironment in solution. Figure 1.12 shows an illustration of various capping ligands used to protect of QD surfaces.

For bio-imaging applications, the most popular capping agents are amphiphilic copolymers. Through functionalization with copolymers and specific antibodies, QDs can be used to target cell receptors [174]. Furthermore, QDs exhibit enhanced photochemical stability compared to organic fluorophores used in *in-vivo* studies [175]. For example, CdSe/ZnS-QD-stained *Xenopus* embryos showed better photostability than did rhodamine-green-dextran dye-labeled embryonic cells [176]. The photostability of QDs makes them ideal labeling agents for studying various events in living cells [177]. QD labeling permits extended observations of cells under continuous illumination as well as multicolor imaging.

1.5.1 Self-assembly of Colloidal Quantum Dots

Organization of nanocrystals into ordered structures is an important issue related to the integration of QDs into devices that have

24 INTELLIGENT NANOMATERIALS

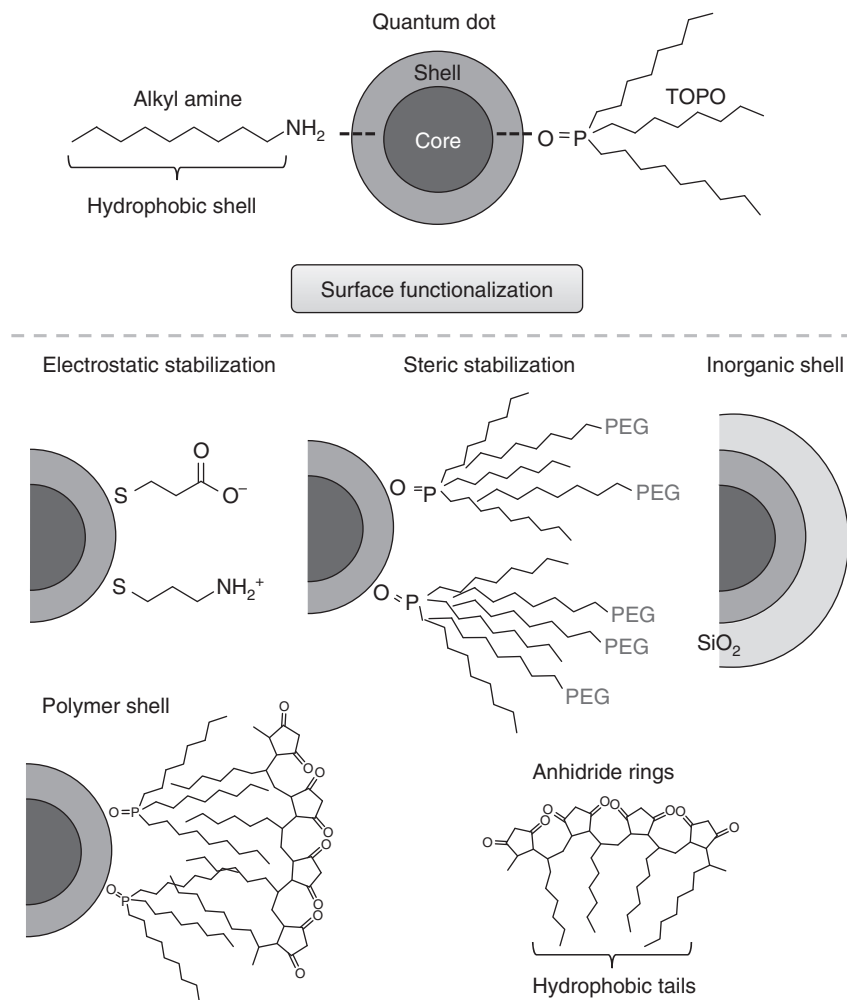


Figure 1.12 Routes for preparation of water-dispersible QDs.

practical applications [178]. In this regard, self-assembly methods have demonstrated great potential for fabrication of photonic, electronic, or magnetoelectronic devices with ordered QDs structures [179]. In this section of the chapter, metal nanoparticles are also reviewed, since the techniques used for their self-assembly are similar to those used for QD self-assembly [180]. The self-assembly of two types of QDs into binary nanocrystal superlattices (BNSL) is described in this section as well [181]. BNSL structures have attracted significant attention because their self-assembly methodology can be used to design metamaterials [182].

The Langmuir–Blodgett (LB) self-assembly technique has recently been found to be useful for covering large-area substrates with nanoparticles. The LB technique has myriad uses, but generally is used for one of two purposes. First, the LB technique can be used to deposit one or more monolayers of QDs onto solid substrates. For example, the LB method has been used by several groups to deposit nanomaterials such as Au [183], Ag [184–186], Pt [187], Fe_3O_4 [188], CdS [189], CdSe [190], and InP [191] onto solid substrates. The LB method offers control over the film thickness and interparticle distances, as well as facile transfer of QDs from liquid phase onto solid substrates. Second, the LB technique can be used to test interfacial properties, such as the surface pressure of a given system. The technique can also be used to observe how QDs arrange themselves as the number of QDs per unit area is varied. Finally, relevant information about the packing of QDs at the air–liquid interface can be obtained from surface pressure–area (π – A) isotherms (Fig. 1.13d).

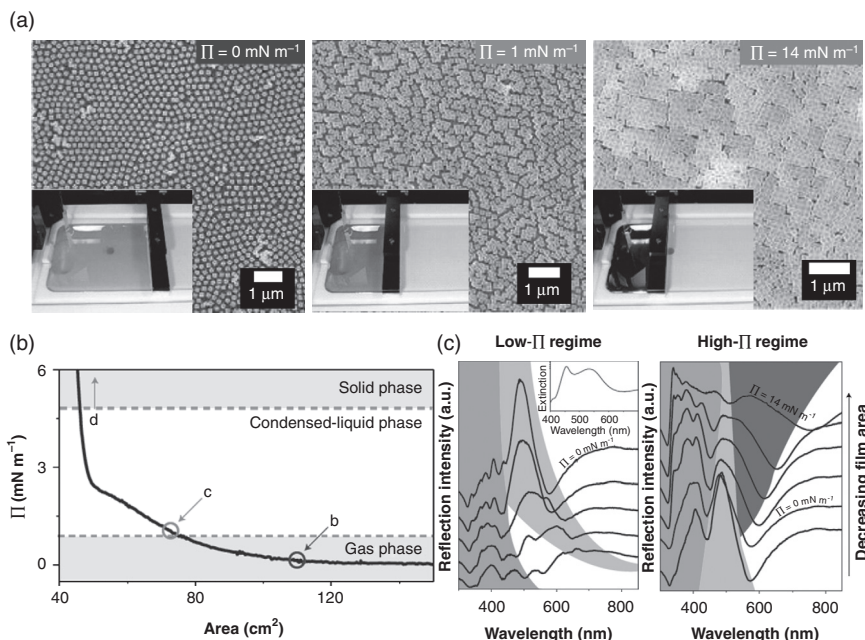


Figure 1.13 (a–c) SEM images of silver nanoparticles transferred onto a solid substrate. Inset images in (a–c) correspond to visual appearances of the films at surface pressures of 0, 1, and 14 mN/m. (d) The surface pressure isotherm of a nanoparticle film. (e) Reflection intensities of the films at different compressions. Reprinted with permission from ref. [192].

26 INTELLIGENT NANOMATERIALS

The isothermal compression of fluid-supported nanoparticles allows for control over the nanoscale assembly by tuning a macroscopic property (i.e., the surface pressure). For example, by changing the surface pressure of a film of Ag nanoparticles, three characteristic phases can be observed [192]: (a) a gas phase above 70 cm^2 , (b) a liquid phase between 50 and 70 cm^2 , and (c) a solid phase below 50 cm^2 . Ordered arrays are achieved at high surface pressures, where the colloidal nanostructures are condensed into a solid film (Fig. 1, 13a, b, c). Moreover, the properties of these films can be studied by reflection spectrometry.

To transfer a monolayer onto a solid substrate, the direction and speed of the substrate's motion must be carefully controlled, along with the surface pressure, composition, temperature, and type of sub-phase used [193, 194]. In a recent study, Weller's group showed that the dipping angle of a substrate into a nanoparticle solution plays a vital role in achieving monolayer films [195]. For example, defect-free monolayers are formed when the substrate-to-liquid angle is about 105° . In a similar fashion, Dong *et al.* studied the effect of sub-phases on the quality of monolayers. For example, when diethylene glycol (DEG) is used as a sub-phase instead of water, the crack-free QD films are formed [196]. The assembly process is favored by DEG's low evaporation rate.

In comparison with the growth of single-component superlattices [197], the self-assembly of binary nanoparticle superlattices (BNSLs) is rather difficult [198]. Despite the calculations accounting for entropy conservation during self-assembly, BNSLs have demonstrated a large variety of possible arrangements. For example, 11 different BNSL structures have been prepared from the same batches of 6.2 nm PbSe QDs and 3.0 nm Pd nanoparticles [199]. Some of these structures were not predicted by entropy conservation rules; prediction of these structures instead requires consideration of additional factors that account for the electrostatic interactions between the nanoparticles. In this regard, tuning the charge state of the nanoparticles could be a way to direct the self-assembly process. Reproducible switching between various lattices has been achieved by introducing molecules like TOPO or carboxylic acids, which can alter the charges of the nanoparticles. Figure 1.14 illustrates possible structures formed when two different types of nanoparticles are mixed together. For example, combining 6.2 nm PbSe and 3.0 nm Pd allows for the formation of a MgZn_2 structure

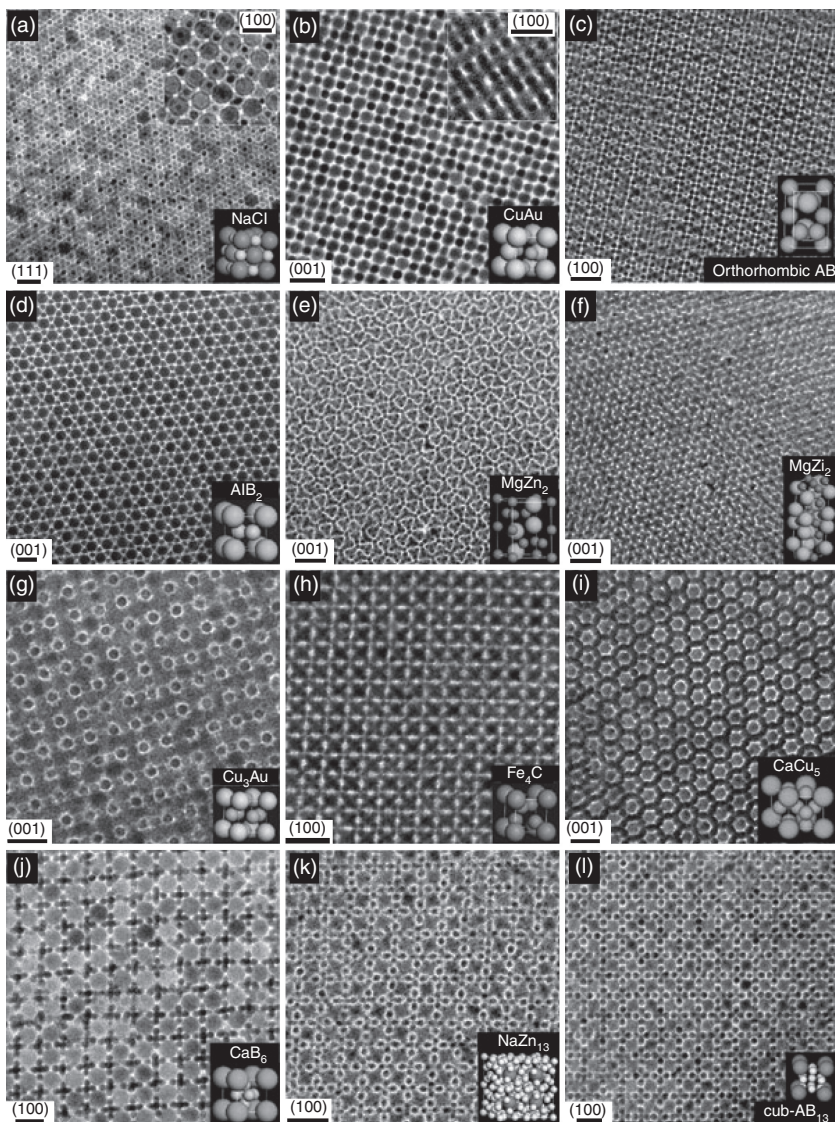


Figure 1.14 TEM images of binary superlattices prepared from different QDs and metal nanoparticles. The types of QDs and metal nanoparticles used to prepare the self-assembled layers are (a) 13.4 nm $\gamma\text{-Fe}_2\text{O}_3$ and 5.0 nm Au, (b) 7.6 nm PbSe and 5.0 nm Au, (c, e, f, h, j, l) PbSe and Pd nanoparticles with various sizes, (d) 6.7 nm PbS and 3.0 nm Pd, (g, k) 7.2 nm PbSe and 4.2 nm Ag, (i) 7.2 nm PbSe and 5.0 nm Au. Scale bars: (a, b, c, e, f, i, j, k, l) 20 nm and (d, g, h) 10 nm. The inset illustrations are modeled unit cells. Reprinted from ref. [199].

28 INTELLIGENT NANOMATERIALS

(Fig. 1.14e). However, similar size nanoparticles self-assemble into an AlB_2 lattice domain in the presence of oleic acid (Fig. 1.14d). The latter result is attributed to the difference in charges in the nanoparticles in the presence of oleic acid.

From a thermodynamic point of view, the Helmholtz free energy (F) of a closed system can be expressed as $F = U - TS$, where U is the internal energy, S is the entropy, and T is the temperature [200]. According to this relationship, T can be used as a weighting factor to estimate the effect of the entropy on the Helmholtz free energy. Additionally, T can be used as a parameter for directing the formation of the desired superlattice. Following this concept, Bodnarchuk *et al.* have demonstrated the effect of temperature on the self-assembly of single and binary nanoparticle superlattices [198]. Figure 1.15 shows BNSL phases assembled at different temperatures from solutions of 7.7 nm PbSe and 3.4 nm Pd nanoparticles. The most common BNSL structure assembled at 25°C is AlB_2 (1:9 ratio). However, at -20°C, 40°C, 85°C, and 100°C, the predominant phases are CuAu and Cu_3Au . Moreover, at a low temperature (<-20°C), these two phases coexist with the NaZn_{13} phase. Variation in the concentration of PbSe to Pd nanoparticles affects the BNSL phase as well. In addition, the type of QDs and metal nanoparticles also affect the self-assembled phases as shown in Fig. 1.14. These observed unique rules for self-assembly constitute a new paradigm in nanomaterials fabrication and could be further exploited for the preparation of intelligent devices.

1.6 Conclusions

In this chapter, we have summarized the most commonly used procedures for preparation of colloidal semiconductor nanocrystals, or quantum dots (QDs). A brief overview of the quantum confinement effect was presented, and the basic photophysical properties of colloidal quantum dots were also described. The discussion of core/shell QDs was emphasized since they are widely prevalent. The functionalization of QDs with molecules and inorganic materials was discussed as it relates to their successful application in various fields. The self-assembly of QDs, which is a challenging and actively evolving area of study, was also reviewed.

In conclusion, QDs will most likely remain a hot research topic during the next decade since they are studied in many different

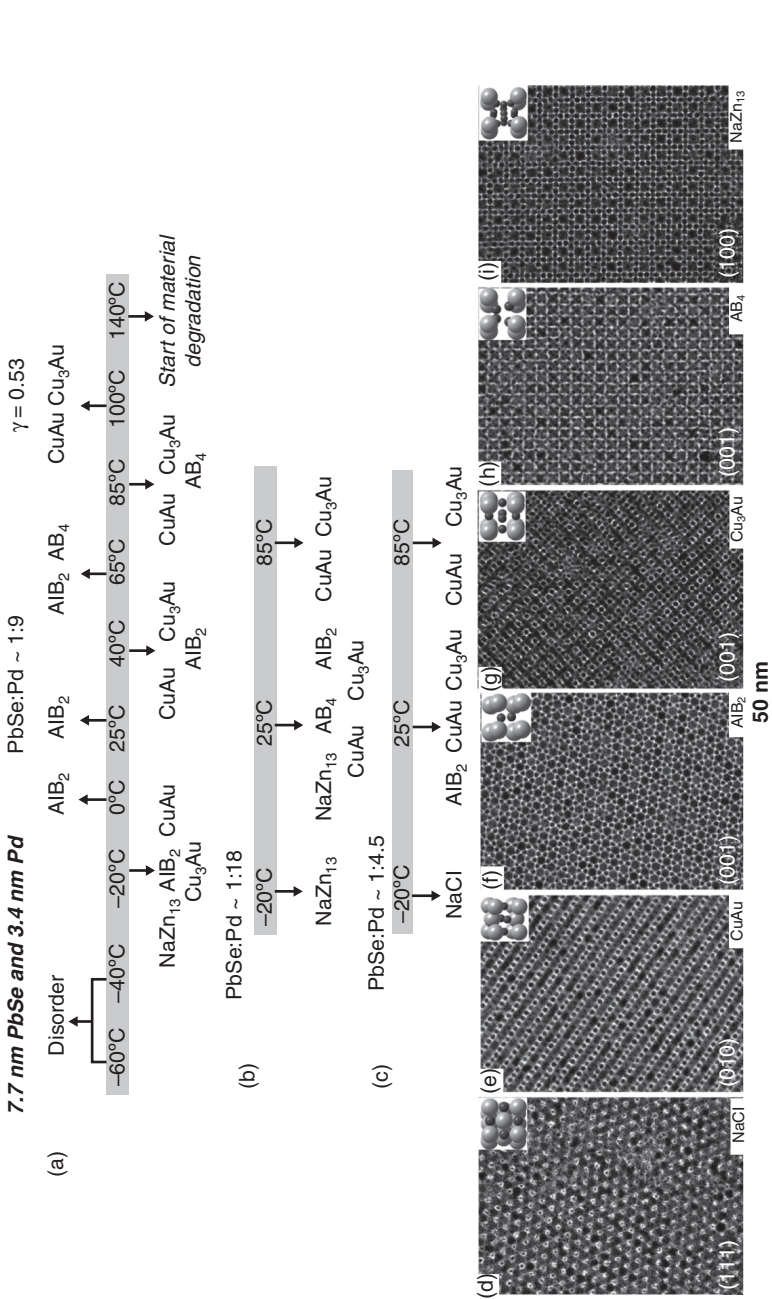


Figure 1.15 (a-c) Scheme illustrating the formation various binary phases between 7.7 nm PbSe and 3.4 nm Pd nanoparticles at different temperatures. (d-i) TEM images representing the following binary phases: (d) NaCl, (e) CuAu, (f) AlB₂, (g) Cu₃Au, (h) AB₄, and (i) NaZn₁₃. Reprinted with permission from ref. [198].

30 INTELLIGENT NANOMATERIALS

scientific disciplines. In the field of biology, QDs have been used as fluorophores because of their high photostability. Moreover, they offer a wide range of wavelengths for emission and photoexcitation. In addition, QDs are also used in photophysical studies aimed at exploring their potential integration into optoelectronic devices.

References

1. X. Michalet, F.F. Pinaud, L.A. Bentolila, J.M. Tsay, S. Doose, J.J. Li, G. Sundaresan, A.M. Wu, S.S. Gambhir, and S. Weiss, *Science*, Vol. 28, p. 538, 2005.
2. C.M. Niemeyer, *Angew. Chem.* Vol. 40, p. 4128, 2001.
3. P. Brown, and P. Kamat, *J. Am. Chem. Soc.*, Vol. 130, p. 8890, 2008.
4. J.M. Caruge, J.E. Halpert, V. Wood, V. Bulovic, and M. Bawendi, *Nature Photonics*, Vol. 2, p. 247, 2008.
5. M. Koneswaran, and R. Narayanaswam, *Sensors and Actuators B*, Vol. 138, p. 104, 2009.
6. A.I. Ekimov, Al.L. Efros, and A.A. Onushchenko, *Sol. State Comm.* Vol. 56, p. 921, 1985.
7. L.E. Brus, *J. Chem. Phys.*, Vol. 79, p. 5566, 1983.
8. N.F. Borelli, and D.W. Smith, *J. Non-Cryst. Sol.*, Vol. 180, p. 25, 1994.
9. E.M. Chan, A.P. Alivisatos, and R.A. Mathies, *J. Am. Chem. Soc.*, Vol. 127, p. 13854, 2005.
10. V.H. Mendez-Garcia, A. Perez-Centeno, M. Lopez-Lopez, *Thin Solid Films*, Vol. 433, p. 63, 2003.
11. M. Gherasimova, J. Su, G. Cui, Z.-Y. Ren, S.-R. Jeon, J. Han, Y. He, Y.-K. Song, A.V. Nurmikko, D. Ciuparu, and L. Pfefferle, *Physica Status Solidi C*, Vol. 2, p. 2361, 2005.
12. Y.-T. Kim, J.H. Han, B.H. Hong, and Y.-U. Kwon, *Adv. Mater.*, Vol. 21, p. 1, 2009.
13. S. Emin, N. Sogoshi, S. Nakabayashi, M. Villeneuve, and C. Dushkin, *J. Photochem. Photobiol. A*, Vol. 207, p. 173, 2009.
14. B. Qin, Z. Zhao, R. Song, S. Shanbhag, and Z. Tang, *Angew. Chem. Int. Ed.*, Vol. 47, p. 1, 2008.
15. S.A. Empedocles, and M.G. Bawendi, *Science*, Vol. 278, p. 2115, 1997.
16. X. Gao, W.C.W. Chan, and S. Nie, *J. Biomedical Optics*, Vol. 7, p. 532, 2002.
17. Q. Sun *et al.*, *ACS Nano*, Vol. 3,737, 2009.
18. R. Freeman, R. Gill, I. Shweky, M. Kotler, U. Banin, and I. Willner, *Angew. Chem. Int. Ed.*, Vol. 47, p. 1, 2008.
19. X. Gao, and S. Nie, *Trends in Biotechnology*, Vol. 21, p. 371, 2003.
20. A. Loukanov, N. Kamasawa, R. Danev, R. Shigemoto, and K. Nagayama, *Ultramicroscopy*, Vol. 110, p. 366, 2010.
21. G.Y.J. Chen, and S.Q. Yao, *The Lancet*, Vol. 364, p. 2001, 2004.
22. Z. Tan *et al.*, *J. Appl. Phys.*, Vol. 105, p. 034312, 2009.
23. D. Bera, L. Qian, T.-K. Tseng, and P. H. Holloway, *Materials*, Vol. 3, p. 2260, 2010.

24. S. Emin, A. Loukanov, M. Wakasa, S. Nakabayashi, and Y. Kaneko, *Chem. Lett.*, Vol. 39, p. 654, 2010.
25. S. V. Nair, S. Sinha, and K.C. Rustagi, *Phys. Rev. B*, Vol. 35, p. 4098, 1987.
26. M.G. Bawendi, M.L. Steigerwald, and L.E. Brus, *Ann. Rev. Phys. Chem.*, Vol. 41, p. 477, 1990.
27. A.L. Efros, M. Rosen, M. Kuno, M. Nirmal, D.J. Norris, and M. Bawendi, *Phys. Rev. B*, Vol. 54, p. 4843, 1996.
28. L.E. Brus, *J. Chem. Phys.*, Vol. 80, p. 4403, 1984.
29. D.J. Norris, "Electronic Structures in Semiconductor Nanocrystals", in V. Klimov, eds., *Semiconductor and Metal Nanocrystals: Synthesis and Electronic and Optical properties*, New York, Marcel Dekker Inc., p. 65–102, 2004.
30. Al.L. Efros, and A.L. Efros, *Sov. Phys. Semicond.*, Vol. 16, p. 772, 1982.
31. S.V. Gaponenko, *Optical Properties of Semiconductor Nanocrystals*, New York, Cambridge University Press, 1998.
32. M.G. Bawendi, M.L. Steigerwald, and L.E. Brus, *Ann. Rev. Phys. Chem.*, Vol. 41, p. 477, 1990.
33. A.V. Rodina, A.Yu. Alekseev, Al.L. Efros, M. Rosen, and B.K. Meyer, *Phys. Rev. B*, Vol. 65, p. 125302, 2002.
34. L. Brus, *IEEE J. Quantum Electron.*, Vol. 22, p. 1909, 1986.
35. Y. Wang, N. Herron, *J. Phys. Chem.*, Vol. 95, p. 525, 1991.
36. P.E. Lippens, and M. Lanoo, *Phys. Rev. B*, Vol. 41, p. 6079, 1990.
37. Y. Masumoto, and K. Sonobe, *Phys. Rev. B*, Vol. 56, p. 9734, 1997.
38. C. Dushkin, S. Saita, K. Yoshie, and Y. Yamaguchi, *Adv. Colloid Interface Sci.*, Vol. 88, p. 37, 2000.
39. V.I. Klimov, "Charge Carrier Dynamics and Optical Gain in Nanocrystal Quantum Dots", in V. Klimov, eds., *Semiconductor and Metal Nanocrystals: Synthesis and Electronic and Optical Properties*, New York, Marcel Dekker Inc., p. 159–213, 2004.
40. D.J. Norris, and M.G. Bawendi, *Phys. Rev. B*, Vol. 53, p. 338, 1996.
41. G.B. Grigoryan, E.M. Kazaryan, A.L. Efros, and T.V. Yazeva, *Sov. Phys. Solid State*, Vol. 32, p. 1031, 1990.
42. U. Woggon, *Optical Properties of Semiconductor Quantum Dots*, Springer Tracts in Modern Physics, Berlin-Heidelberg, Springer-Verlag, 1997.
43. Al.L. Efros, and A.V. Rodina, *Phys. Rev. B*, Vol. 47, p. 10005, 1993.
44. P.D. J. Calcott, K.J. Nash, L.T. Canham, M.J. Kane, and D. Brumhead, *J. Luminescence*, Vol. 57, p. 257, 1993.
45. D. Langevin, "Structure of Reversed Micelles", in M.P. Pilani, eds., *Structure and Reactivity in Reverse Micelles*, Elsevier Science Publishers B.V., pp. 13–43, 1989.
46. E.P. Melo, P. Fojah, J.M. Cabral, and S.B. Petersen, *Chem. Phys. Lipids*, Vol. 106, 181, 2000.
47. F. Pitre, and M.P. Pilani, *Prog. Colloid Polym. Sci.*, Vol. 93, p. 333, 1993.
48. B. Simmons, V. Agarwal, G. McPherson, V. John, and A. Bose, *Langmuir*, Vol. 18, p. 8345, 2002.
49. T. Kinugasa, A. Kondo, S. Nishimura, Y. Miyauchi, Y. Nishii, K. Watanabe, and H. Takeuchi, *Colloids and Surfaces A*, Vol. 204, p. 193, 2002.
50. M.L. Steigerwald, and L.E. Brus, "Synthesis and Surface Reactions of Semiconductor Crystallite Clusters in Reverse Micelle Media", in M.P. Pilani,

32 INTELLIGENT NANOMATERIALS

- eds., *Structure and Reactivity in Reverse Micelles*, Elsevier Science Publishers B.V., pp. 189–197, 1989.
51. B.H. Robinson, A.N. Khan-Lodhi, and T. Towery, “Microparticle Synthesis and Characterization in Reverse Micelles”, in M.P. Pileni, eds., *Structure and Reactivity in Reverse Micelles*, Elsevier Science Publishers B.V., pp. 189–197, 1989.
 52. M. Meyer, C. Walberg, K. Kurihara, and J.H. Fendler, *J. Chem. Soc. Chem. Commun.*, Vol. 90, 1984.
 53. S.M. Emin, C.D. Dushkin, S. Nakabayashi, and E. Adachi, *Centr. European J. Chem.*, Vol. 5, 590, 2007.
 54. P. Lianos, and J.K. Thomas, *Chem. Phys. Lett.*, Vol. 125, p. 299, 1986.
 55. W. Xu, and D.L. Akins, *Mater. Lett.*, Vol. 58, p. 2623, 2004.
 56. C. Petit, and M.P. Pileni, *J. Phys. Chem.*, Vol. 92, p. 2282, 1988.
 57. N. Chandrasekharam, and P.V. Kamat, *Res. Chem. Intermed.*, Vol. 28, p. 847, 2002.
 58. J. Eastoe, and A.R. Cox, *Colloids and Surfaces A*, Vol. 101, p. 63, 1995.
 59. A.R. Loukanov, C.D. Dushkin, K.I. Papazova, A.V. Kirov, M.V. Abrashev, and E. Adachi, *Colloids and Surfaces A*, Vol. 245, p. 9, 2004.
 60. T. Rajh, O. Micic, and A.J. Nozik, *J. Phys. Chem.*, Vol. 97, p. 11999, 1993.
 61. M. Gao, S. Kirstein, H. Mohwald, A.L. Rogach, A. Kornowski, A. Eychmüller, and H. Weller, *J. Phys. Chem. B*, Vol. 102, p. 8360, 1998.
 62. A.L. Rogach, T. Franzl, T.A. Klar, J. Feldmann, N. Gaponik, V. Lesnyak, A. Shavel, A. Eychmüller, Y.P. Rakovich, and J.F. Donegan, *J. Phys. Chem. C*, Vol. 111, p. 14628, 2007.
 63. N.N. Mamedova, N.A. Kotov, A.L. Rogach, and J. Studer, *Nano Lett.*, Vol. 1, p. 281, 2001.
 64. H. Qian, C. Dong, J. Weng, and J. Ren, *Small*, Vol. 2, p. 747, 2006.
 65. Z. Tang, Z. Zhang, Y. Wang, S.C. Glotzer, and N.A. Kotov, *Science*, Vol. 314, p. 274, 2006.
 66. Z. Fang, L. Liu, L. Xu, X. Yin, and X. Zhou, *Nanotechnology*, Vol. 19, p. 235603, 2008.
 67. C. Wang, Q. Ma, and X. Su, *J. Nanosci. Nanotechnol.*, Vol. 8, p. 4408, 2008.
 68. Y.F. Liu, and J.S. Yu, *J. Colloid Interface Sci.*, Vol. 351, p. 1, 2010.
 69. A. Rogach, S. Kershaw, M. Burt, M. Harrison, A. Kornowski, A. Eychmüller, and H. Weller, *Adv. Mater.*, Vol. 11, p. 552, 1999.
 70. Z. Fang, Y. Li, H. Zhang, X. Zhong, and L. Zhu, *J. Phys. Chem. C*, Vol. 113, p. 14145, 2009.
 71. T. Vossmeier, L. Katsikas, M. Giersig, I. G. Popovic, K. Diesner, A. Chemseddine, A. Eychmüller, and H. Weller, *J. Phys. Chem.*, Vol. 98, p. 7665, 1994.
 72. Y.-S. Xia, and C.-Q. Zhu, *Mater. Lett.*, Vol. 62, p. 2103, 2008.
 73. M.T. Harrison, S.V. Kershaw, M.G. Burt, A. Eychmüller, H. Weller, and A.L. Rogach, *Mat. Sci. Eng. B*, Vol. 69, p. 355, 2000.
 74. A. Rogach, S. Kershaw, M. Burt, M. Harrison, A. Kornowski, A. Eychmüller, and H. Weller, *Adv. Mater.*, Vol. 11, p. 552, 1999.
 75. N. Gaponik, and A.L. Rogach, “Aqueous synthesis of semiconductor nanocrystals”, in A.L. Rogach, eds., *Semiconductor nanocrystal quantum dots*, Springer-Verlag, Wien, pp. 73–99, 2008.
 76. H. Zhang, Z. Zhou, B. Yang, and M. Gao, *J. Phys. Chem. B*, Vol. 107, p. 8, 2003.

77. N. Gaponik, D.V. Talapin, A.L. Rogach, K. Hoppe, E.V. Shevchenko, A. Kornowski, A. Eychmüller, and H. Weller, *J. Phys. Chem. B*, Vol. 106, p. 7177, 2002.
78. A.D. Maynard, R.J. Aitken, T. Butz, V. Colvin, K. Donaldson, G. Oberdoerster, M.A. Philbert, J. Ryan, A. Seaton, V. Stone, S.S. Tinkle, L. Tran, N.J. Walker, and D.B. Warheit, *Nature*, Vol. 444, p. 267, 2006.
79. D-W. Deng, J-S. Yu, and Y. Pan, *J. Colloid Interf. Sci.*, Vol. 299, p. 225, 2006.
80. P. Reiss, *New J. Chem.*, Vol. 31, p. 1743, 2007.
81. N. Murase, and M. Gao, *Mater. Lett.*, Vol. 58, p. 3898, 2004.
82. A. Shavel, N. Gaponik, and A. Eychmüller, *J. Phys. Chem. B*, Vol. 108, p. 5905, 2004.
83. C. Bertoni, D. Gallardo, S. Dunn, N. Gaponik, and A. Eychmüller, *Appl. Phys. Lett.*, Vol. 90, p. 034107, 2007.
84. N. Gaponik, and A.L. Rogach, *Phys. Chem. Chem. Phys.*, Vol. 12, p. 8685, 2010.
85. M.B.O. Dabbousi, J. Rodriguez-Viejo, F.V. Mikulec, J.R. Heine, H. Mattoussi, R. Ober, K.F. Jensen, M.G. Bawendi, *J. Phys. Chem. B*, Vol. 101, p. 9463, 1997.
86. C.B. Murray, D.J. Norris, M.G. Bawendi, *J. Am. Chem. Soc.*, Vol. 115, p. 8706, 1993.
87. G.Y. Yordanov, H. Yoshimura, and C.D. Dushkin, *Colloid Polym. Sci.*, Vol. 286, p. 1097, 2008.
88. N. Pradhan, D. Reifsnyder, R. Xie, J. Aldana, and X. Peng, *J. Am. Chem. Soc.*, Vol. 129, p. 9500, 2007.
89. Y.A. Yang, H. Wu, K.R. Williams, and Y.C. Cao, *Angew. Chem. Int. Ed.*, Vol. 44, p. 6712, 2005.
90. W. Yu, and X. Peng, *Angew. Chem. Int. Edit.*, Vol. 41, p. 2368, 2002.
91. C.I. Ratcliffe, K. Yu, J.A. Ripmeester, Md.B. Zaman, C. Badarau, and S. Singh, *Phys. Chem. Chem. Phys.*, Vol. 8, p. 3510, 2006.
92. A.M. Munro, I.J.-L. Plante, M.S. Ng, and D.S. Ginger, *J. Phys. Chem. C*, Vol. 111, p. 6221, 2007.
93. J.S. Steckel, J.P. Zimmer, S. Coe-Sullivan, N.E. Stott, V. Bulovic, and M.G. Bawendi, *Angew. Chem. Int. Ed.*, Vol. 43, p. 2154, 2004.
94. M.A. Hines, and P. Guyot-Sionnest, *J. Phys. Chem.*, Vol. 100, p. 468, 1996.
95. R. Freeman, T. Finder, L. Bahshi, and I. Willner, *Nano Lett.*, Vol. 9, p. 2073, 2009.
96. S. Chaudhary, and M. Ozkan, *Appl. Phys. Lett.*, Vol. 84, p. 2926, 2004.
97. J. Zhao, J.A. Bardecker, A.M. Munro, M.S. Liu, Y. Niu, I.-K. Ding, J. Luo, B. Chen, A.K.-Y. Jen, and D.S. Ginger, *Nano Lett.*, Vol. 6, p. 463, 2006.
98. C.-Y. Chen, C.-T. Cheng, C.-W. Lai, Y.-H. Hu, P.-T. Chou, Y.-H. Chou, and H.T. Chiu, *Small*, Vol. 1, p. 1215, 2005.
99. A.W. Schill, C.S. Gaddis, W. Qian, M.A. El-Sayed, Y.C. Valeria, T. Milam, and K. Sandhage, *Nano Lett.*, Vol. 6, p. 1940, 2006.
100. V. Sholin, A.J. Breeze, I.E. Anderson, Y. Sahoo, D. Reddy, and S.A. Carter, *Sol. Energy Mater. Sol. Cells*, Vol. 92, p. 1706, 2008.
101. A.I. Ekimov, and A.A. Onuschenko, *JETP Letters*, Vol. 34, p. 345, 1981.
102. H. Zhang, B. Gilbert, F. Huang, and J.F. Banfield, *Nature*, Vol. 424, p. 1025, 2003.
103. M.A. Hines, and P. Guyot-Sionnest, *J. Phys. Chem. B*, Vol. 102, p. 3655, 1998.
104. J.R. Lakowicz, I. Gryczynski, Z. Gryczynski, and C.J. Murphy, *J. Phys. Chem. B*, Vol. 103, p. 7616, 1999.

34 INTELLIGENT NANOMATERIALS

105. X. Peng, L. Manna, W. Yang, J. Wickham, E. Scher, A. Kadavanich, and A.P. Alivisatos, *Nature*, Vol. 404, p. 59, 2000.
106. B. Xing, W. Li, and K. Sun, *Mater. Lett.*, Vol. 62, p. 3178, 2008.
107. S. Ogawa, K. Hu, F.-R.F. Fan, and A.J. Bard, *J. Phys. Chem. B*, Vol. 101, p. 5707, 1997.
108. Z. Hens, I. Moreels, and J.C. Martins, *Chem. Phys. Chem.*, Vol. 6, p. 2578, 2005.
109. M.A. Olshavsky, A.N. Goldstein, and A.P. Alivisatos, *J. Am. Chem. Soc.*, Vol. 112, p. 9438, 1990.
110. R. Koole, P. Schapotschnikow, C.M. Donega, T.J.H. Vlugt, and A. Meijerink, *ACS Nano*, Vol. 2, p. 1703, 2008.
111. J. Volker, X. Zhou, X. Ma, S. Flessa, H. Lin, M. Schmittel, and A. Mews, *Angew. Chem. Int. Ed.*, Vol. 49, p. 6865, 2010.
112. A.M. Smith, and S. Nie, *J. Am. Chem. Soc.*, Vol. 133, p. 24, 2011.
113. R.E. Bailey, and S. Nie, *J. Am. Chem. Soc.*, Vol. 125, p. 7100, 2003.
114. D. Kim, A. Nabeshima, and M. Nakayama, *Jpn. J. Appl. Phys.*, Vol. 41, p. 5064, 2002.
115. D. Kim, S. Okahara, K. Shimura, and M. Nakayama, *J. Phys. Chem. C*, Vol. 113, p. 7015, 2009.
116. X.B. Zhang, and S.K. Hark, *J. Crystal Growth*, Vol. 208, p. 231, 2000.
117. A. Becker, C. Hessenius, K. Licha, B. Ebert, U. Sukowski, W. Semmler, B. Wiedenmann, and C. Grotzinger, *Nat. Biotechnol.*, Vol. 19, p. 327, 2001.
118. S. McWhorter, and A.A. Soper, *Electrophoresis*, Vol. 21, p. 1267, 2000.
119. L. Qu, and X.G. Peng, *J. Am. Chem. Soc.*, Vol. 124, p. 2049, 2002.
120. L.P. Balet, S.A. Ivanov, A. Piryatinski, M. Achermann, and V.I. Klimov, *Nano Lett.*, Vol. 4, p. 1485, 2004.
121. P. Reiss, M. Protiere, and L. Li, *Small*, Vol. 5, p. 154, 2009.
122. S. Jun, and E. Jang, *Chem. Comm.*, Vol. 36, p. 4616, 2005.
123. M. Schlamp, X. Peng, and A.P. Alivisatos, *J. Appl. Phys.*, Vol. 82, p. 5837, 1997.
124. R. Vinayakan, T. Shanmugapriya, Pratheesh V. Nair, P. Ramamurthy, and K. George Thomas, *J. Phys. Chem. C*, Vol. 111, p. 10146, 2007.
125. Z. Yu, L. Guo, H. Du, T. Krauss, and J. Silcox, *Nano Lett.*, Vol. 5, p. 565, 2005.
126. D. Bera, L. Qian, and P.H. Holloway, "Phosphor Quantum Dots", in A. Kitai, eds., *Luminescent Materials and Applications*, John Wiley&Sons Ltd., pp. 19–65, 2008.
127. Y. Nonoguchi, T. Nakashima, and T. Kawai, *Small*, Vol. 5, p. 2403, 2009.
128. S. Wang, and L. Wang, *J. Phys. Chem. Lett.*, Vol. 2, p. 1, 2010.
129. K. Yu, B. Zaman, S. Romanova, S. Romanova, D. Wang, and J.A. Ripmeester, *Small*, Vol. 1, p. 332, 2005.
130. Q. Zheng, X. Kong, Y. Sun, Y. Zhang, L. Tu, J. Zhao, and H. Zhang, *J. Phys. Chem. C*, Vol. 112, p. 8587, 2008.
131. E. Holder, N. Tessler, and A.L. Rogach, *J. Mater. Chem.*, Vol. 18, p. 1064, 2008.
132. H.S. Zhou, H. Sasahara, I. Honma, H. Komiyama, and J.W. Haus, *Chem. Mater.*, Vol. 6, p. 1534, 1994.
133. Y.W. Cao, and U. Banin, *Angew. Chem. Int. Ed.*, Vol. 38, p. 3692, 1999.
134. C.H. Liu, *Opto-Electron. Rev.*, Vol. 11, p. 1, 2003.
135. Y. Zhang, Y. Li, and X. Yan, *Small*, Vol. 5, p. 185, 2009.
136. A. Smith, A.M. Mohs, and S. Nie, *Nature Nanotech.*, Vol. 4, p. 56, 2009.

137. S. Kim, B. Fisher, H.-J. Eisler, and M. Bawendi, *J. Am. Chem. Soc.*, Vol. 125, p. 11466, 2003.
138. M. Dahan, T. Laurence, F. Pinaud, D.S. Chemia, A.P. Alivisatos, M. Sauer, and S. Weiss, *Opt. Lett.*, Vol. 26, p. 825, 2001.
139. M.-K. So, C. Xu, A.M. Loening, S.S. Gamhir, and J. Rao, *Nature Biotech.*, Vol. 24, p. 339, 2006.
140. H. Borchert, D. Dorfs, C. McGinley, S. Adam, T. Moller, H. Weller, and A. Eychmuller, *J. Phys. Chem. B*, Vol. 107, p. 7486, 2003.
141. H.V. Demir, S. Nizamoglu, E. Mutlugun, T. Ozel, S. Sapra, N. Gaponik, and A. Eychmuller, *Nanotechnology*, Vol. 19, p. 335203, 2008.
142. C.-Y. Huang, Y.-K. Su, Y.-C. Chen, P.-C Tsai, C.-T. Wan, W.-L. and Li, *Electron Device Letters*, Vol. 29, p. 711, 2008.
143. L. Cao, S. Huang, and E. Shulin, *J. Coll. Interface Sci.*, Vol. 273, p. 478, 2004.
144. D. Schooss, A. Mews, A. Eychmuller, and H. Weller, *Phys. Rev. B*, Vol. 49, p. 17072, 1994.
145. G.W. Bryant, *Phys. Rev. B*, Vol. 52, p. 16997, 1995.
146. D. Bataglia, B. Blackman, and X. Peng, *J. Am. Chem. Soc.*, Vol. 127, p. 10889, 2005.
147. R. Kostic, and D. Stojanovic, *Acta Physica Polonica A*, Vol. 116, p. 598, 2009.
148. V.F. Kamalov, R. Little, S.L. Logunov, and M.A. El-Sayed, *J. Phys. Chem.*, Vol. 100, p. 6381, 1996.
149. A. Mews, A.V. Kadavanich, A.A. Guzelian, and A.P. Alivisatos, *Phys. Rev. B*, Vol. 53, p. 13242, 1996.
150. E. Lifshitz, H. Porteanu, A. Golzman, H. Weller, M. Pflughoeft, and A. Eychmuller, *J. Phys. Chem. B*, Vol. 103, p. 6870, 1999.
151. S. Nizamoglu, E. Mutlugun, T. Ozel, H.V. Demir, S. Sapra, N. Gaponik, and A. Eychmuller, *Appl. Phys. Lett.*, Vol. 92, p. 113110, 2008.
152. E. Lifshitz, H. Porteanu, A. Golzman, H. Weller, M. Pflughoeft, and A. Eychmuller, *J. Phys. Chem. B*, Vol. 103, p. 6870, 1999.
153. D.J. Norris, A.L. Efros, and S.C. Erwin, *Science*, Vol. 319, p. 1779, 2008.
154. T. Gurung, S. Mackowski, H.E. Jackson, L.M. Smith, W. Heiss, J. Kossut, and G. Karczewski, *J. Appl. Phys.*, Vol. 96, p. 7408, 2004.
155. S.M. Emin, N. Sogoshi, S. Nakabayashi, T. Fujihara, and C.D. Dushkin, *J. Phys. Chem. C*, Vol. 113, p. 3998, 2009.
156. R. Beaulac, P.I. Archer, X. Liu, S. Lee, G.M. Salley, M. Dobrowolska, J. K. Furdyna, and D.R. Gamelin, *Nano Lett.*, Vol. 8, p. 1197, 2008.
157. N. Pradhan, D. Goorskey, J. Thessing, and X. Peng, *J. Am. Chem. Soc.*, Vol. 127, p. 17586, 2005.
158. N.S. Norberg, G.L. Parks, G.M. Salley, and D.R. Gamelin, *J. Am. Chem. Soc.*, Vol. 128, p. 13195, 2006.
159. T.A. Kennedy, E.R. Glaser, P.B. Kelin, and R.N. Bhargava, *Phys. Rev. B*, Vol. 52, p. 14356, 1995.
160. S. Jana, B.B. Srivastava, S. Acharya, P.K. Santra, N.R. Jana, D.D. Sarma, and N. Pradhan, *Chem. Comm.*, Vol. 46, p. 2853, 2010.
161. L. Levy, N. Feltin, D. Ingert, and M.P. Pilani, *J. Phys. Chem. B*, Vol. 101, p. 9153, 1997.
162. T. Kuroda, H. Ito, F. Minami, and H. Akinaga, *J. Lumines.*, Vol. 72, p. 106, 1997.

36 INTELLIGENT NANOMATERIALS

163. V.A. Vlaskin, N. Janssen, J. van Rijssel, R. Beaulac, and D. R. Gamelin, *Nano Lett.*, Vol. 10, p. 3670, 2010.
164. R. Beaulac, L. Schneider, P.I. Archer, G. Bacher, and D.R. Gamelin, *Science*, Vol. 325, p. 973, 2009.
165. A.M. Derfus, W.C.W. Chan, S.N. Bhatia, *Nano Lett.*, Vol. 4, p. 11, 2004.
166. A.K. Rath, S. Bhaumik, and A.J. Pal, *Appl. Phys. Lett.*, Vol. 97, p. 113502, 2010.
167. W.C.W. Chan, and S. Nie, *Science*, Vol. 281, p. 2016, 1998.
168. X. Gao, Y. Cui, R.M. Levenson, L.W.K. Chung, *Nature Biotechnol.*, Vol. 22, p. 969, 2004.
169. S. Kim, and M.G. Bawendi, *J. Am. Chem. Soc.*, Vol. 125, p. 14652, 2003.
170. F. Osaki, T. Kanamori, S. Sando, T. Sera, and Y. Aoyama, *J. Am. Chem. Soc.*, Vol. 126, p. 6520, 2004.
171. W.J. Park *et al.*, *Chem. Mater.*, Vol. 14, p. 2113, 2002.
172. U. Resch-Genger, M. Grabolle, S. Cavaliere-Jaricot, R. Nitschke, and T. Nann, *Nat. Methods*, 5, p. 763, 2008.
173. S. Mazumder, R. Dey, M.K. Mitra, S. Mukherjee, and G.C. Das, *J. Nanotechnology*, doi: 10.1155/2009/815734.
174. Y. Xing *et al.*, *Nat. Protoc.*, Vol. 2, p. 1152, 2007.
175. I.L. Medintz, H.T. Uyeda, E.R. Goldman, and H. Mattoussi, *Nat. Mater.*, Vol. 4, p. 435, 2005.
176. B. Dubertret, P. Skourides, D.J. Norris, V. Noireaux, A.H. Brivanlou, and A. Libchaber, *Science*, Vol. 298, p. 1759, 2002.
177. J.K. Jaiswal, H. Mattoussi, J.M. Mauro, and S.M. Simon, *Nature Biotechnol.*, Vol. 21, p. 47, 2003.
178. K. Lambert, L. Witterbrood, I. Moreels, D. Deresmes, B. Grandidier, and Z. Hens, *J. Colloid Interf. Sci.*, Vol. 300, p. 597, 2006.
179. M.-P. Pilani, *Acc. Chem. Res.*, Vol. 40, p.685, 2007.
180. H. Song, F. Kim, S. Connor, G.A. Somorjai, and P. Yang, *J. Phys. Chem. B*, Vol. 109, p. 188, 2005.
181. A.E. Saunders, and B.A. Korgel, *Chem. Phys. Chem.*, Vol. 6, p. 61, 2005.
182. F.X. Redl, K.S. Cho, C.B. Murray, and S. O'Brien, *Nature*, Vol. 423, p. 968, 2003.
183. J.R. Heath, C.M. Knobler, and D.V. Leff, *J. Phys. Chem. B*, Vol. 101, p. 189, 1997.
184. C.P. Collier, R.J. Saykally, J.J. Shiang, S.E. Henrichs, and J.R. Heath, *Science*, Vol. 277, p. 1978, 1997.
185. C. Xue, X. Chen, S.J. Hurst, and C.A. Mirkin, *Adv. Mater.*, Vol. 19, p. 4071, 2007.
186. A.Tao, P. Sinsermsuksakul, and P. Yang, *Nat. Nanotechnology*, Vol. 2, p. 435, 2007.
187. H. Song, F. Kim, S. Connor, G.A. Somorjai, and P. Yang, *J. Phys. Chem. B*, Vol. 109, p. 188, 2005.
188. T. Fried, G. Shemer, and G. Markovich, *Adv. Mater.*, Vol. 13, p. 1158, 2001.
189. C. Damle, A. Gole, and M. Sastry, *J. Mat. Chem.*, Vol. 10, p. 1389, 2000.
190. B.O. Dabbousi, C.B. Murray, M.F. Rubner, and M.G. Bawendi, *Chem. Mater.*, Vol. 6, p. 216, 1994.
191. K. Lambert, L. Witterbrood, I. Moreels, D. Deresmes, B. Grandidier, and Z. Hens, *J. Colloid Interf. Sci.*, Vol. 300, p. 597, 2006.
192. A.R. Tao, J. Huang, and P. Yang, *Accounts of Chemical Research*, Vol. 41, p. 1662, 2008.

SYNTHESIS, CHARACTERIZATION, AND SELF-ASSEMBLY 37

193. J. Huang, R. Fan, S. Connor, and P. Yang, *Angew. Chem. Int. Ed.*, Vol. 46, p. 2414, 2007.
194. K.M. Gattas-Asfura, C.A. Constantine, M.J. Lynn, D.A. Thimann, X.Ji, and R.M. Leblanc, *J. Am. Chem. Soc.*, Vol. 127, p. 14640, 2005.
195. V. Aleksandrovic, D. Greshnykh, I. Randjelovic, A. Fromsdorf, A. Kornowski, S. Volkher Roth, C. Klinke, and H. Weller, *ACS Nano*, Vol. 2, p. 1123, 2008.
196. A. Dong, J. Chen, P.M. Vora, J.M. Kikkawa, and C.B. Murray, *Nature*, Vol. 466, p. 474, 2010.
197. Y. Wang, Q. Dai, B. Zou, W.W. Yu, B. Liu, and G. Zou, *Langmuir*, Vol. 26, 19129, 2010.
198. M.I. Bodnarchuk, M.V. Kovalenko, W. Heiss, and D.V. Talapin, *J. Am. Chem. Soc.*, Vol. 132, p. 11967, 2010.
199. E.V. Shevchenko, D.V. Talapin, N.A. Kotov, S. O'Brein, and C.B. Murray, *Nature*, Vol. 439, p. 55, 2006.
200. D. Frenkel, B.M. Mulder, and J.P. McTague, *Phys. Rev. Lett.*, Vol. 52, p. 287, 1984.

